Wind Energy Harnessing in a Railway Infrastructure: Converter Topology and Control Proposal

Oier Oñederra [1,*], **Francisco Javier Asensio** [2], **Gaizka Saldaña** [2], **José Ignacio San Martín** [2] **and Inmaculada Zamora** [1]

[1] Department of Electrical Engineering, Engineering School of Bilbao, University of the Basque Country (UPV/EHU), 48013 Bilbao, Bizkaia, Spain; inmaculada.zamora@ehu.eus
[2] Department of Electrical Engineering, Engineering School of Gipuzkoa, University of the Basque Country (UPV/EHU), 20600 Eibar, Gipuzkoa, Spain; franciscojavier.asensio@ehu.eus (F.J.A.); gaizka.saldana@ehu.eus (G.S.); joseignacio.sanmartin@ehu.eus (J.I.S.M.)
* Correspondence: oier.onederra@ehu.eus

check for updates

Abstract: Long distances in the vicinities of railways are not exploited in terms of wind energy. This paper presents a scalable power electronics approach, aimed to harness the wind potential in a railway infrastructure. The key aspect of this proposal relies on both using the wind energy in the location, and the displaced air mass during the movement of a train along the railway, in order to produce electrical energy. Vertical Axis Wind Turbines (VAWT) are used in order to take advantage of the wind power, and widely used and well-known power converter techniques to accomplish the goal, showing MPPT techniques, parallelization of converters and power delivery with a Solid State Transformer (SST). Results are shown according simulations of the whole system, with and without train activity, resulting that 30.6 MWh of the energy could be generated without the train, and the energy generated with the assistance of the train could reach 32.3 MWh a year. Concluding that almost the 10% of the energy could be provided by the assistance of the train.

Keywords: wind; railway; MPPT; MVDC; DAB

1. Introduction

Nowadays, there is a global awareness of the existing energetic problem and the concern about environmental issues, which both lead to taking advantage of renewable energy sources, and are intensified by the economic crises of the last few years.

In 2017, worldwide total primary energy supply reached 13,972 *Mtoe*, which is translated into an increase 2.5 times higher compared to 1971. Although the total amount has changed, its structure has not significantly changed, fossil fuels being the leading origin, with an evolution from 87% in 1971 to 81% in 2017. Among technologies in power generation, coal accounted the largest share, 38.5% in 2017 [1].

Concerning emissions, the transportation sector is considered critical since it is responsible of the 24% of direct CO_2 emissions from fuel combustion [2], and one of the worldwide sectors where CO_2 emissions are on the rise. It has to be noted that the increasing trend is about 0.5% in 2019, which is quite significantly lower than the 1.9% annual increase from 2000 on. This improvement is majorly due to efficiency improvements, electrification and greater use of biofuels [2–4]. Note that transport electrification has to be performed together with power generation decarbonization, since, otherwise, global emissions could increase. In this sense, the decarbonization of energy, especially by increasing penetration of renewable energy sources and transport electrification are recognized as key policies towards a more sustainable world [5].

Regarding rail transportation, it comprises from urban metros to high-speed rail services, and it is considered one of the most efficient transport modes, currently it is responsible for the 9% of total passenger movement and 7% of total freight [2]. An important improvement in the efficiency of the railway systems has come through the regenerative braking of traction vehicles, deliverying part of kinetic energy while breaking or slowing down the train to the catenary [5,6]. However, there is still room for improvement in the transportation sector, which could be carried out by renewable energies integration, since transport electrification only shifts the problem to generation technologies and power related sector. In this context, renewable energy sources are gaining presence in industry and public infrastructure [7]. In this sense, the improvement in efficiency in transportation systems is one of the issues to deal with, and the railway system is part of it. In fact, the railway system is one of the most suitable transport systems with renewable energies, especially wind energy.

The idea of generating electric energy in the nearby of railways is not new. Some ideas use the piezoelectric properties of some materials to supply part of the train station loads [8], and others, suggest the availability of the wind energy due to the displacement of air mass while the train circulates inside a tunnel [9–12]. However, despite the fact that the effect of speed is magnified inside a tunnel, when there is no train in motion, the wind turbines do not produce energy, thus reducing its utilization factor and thus increasing the payback of the system. In other research works, researchers have demonstrated the technical viability with two couple wind turbine types, in the mW range, just to feed monitoring sensors inside a tunnel [13]. Other examples [12] focus in including variations in wind turbine construction so it can vary its height according to its needs, but only performs a simple and theoretical analysis of the wind turbine performance, without explaining power conditioning scheme and its optimal integration.

This paper proposes a wind generation layout (Figure 1) and a power converter topology selection with control (Figure 2) in the field of railway infrastructures. This work tries to quantify the energy generated both with the local wind and the wind generated by train movement, using proposed power converters to achieve scalability and redundancy.
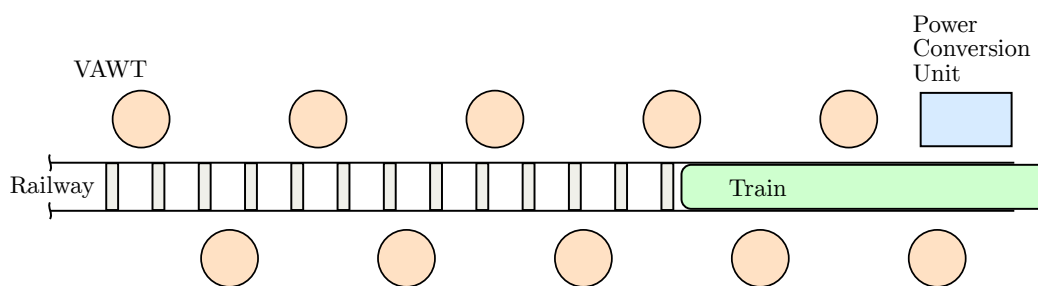

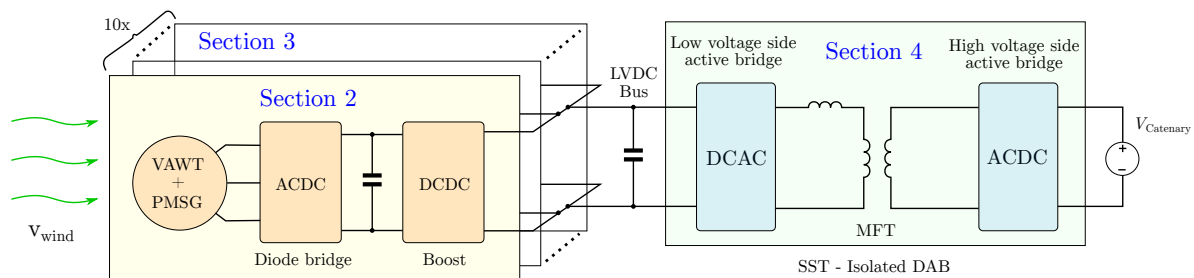**Figure 1.** Layout of the 10 VAWTs along the railway.

Figure 2. Power conversion system.

To show this proposal, this paper is organized as follows: in Section 2, the wind energy conversion system is shown with the vertical axis wind turbine (VAWT), permanent magnet synchronous generator (PMSG), diode bridge and boost converter. Section 3 describes the parallelization of these converters. The Section 4 shows the delivery of generated power to catenary with the solid-state transformer (SST). In Section 5, some simulations and results are presented, ending with conclusions in Section 6.

2. Wind Energy Conversion

The target of the system is to inject power to the catenary of the railway. So the wind power conversion has several steps and issues to overcome, which is the technical goal of this paper, and the use of the local wind and air mass movement due to train quantization is the other object of this paper.

First of all, wind turbines are defined and located, which are mechanically connected to a PMSG. This PMSG generates three-phase AC currents so an ACDC converter has been connected and implemented a maximum power point algorithm in order to extract the most from the PMSG. This DC output simplifies the parallelization of the converters to add power to the system, which is discussed later.

2.1. Wind Turbine

The location of the wind turbines along the railway has been selected mainly according to be an open area of the railway, and a long enough track between stops. The open area helps to enhance the factor of utilization comparing to a tunnel placement, and the long track enables the high wind speed generated nearby the train (Figure 1). This location has an average wind speed of 5 m/s according to data and interpolations [14]. In order to estimate the wind energy nearby the train, some simulations have been carried out in [14], concluding in a generated wind speed of 7.7 m/s.

In these scenarios VAWTs give advantages over HAWTs mainly in two aspects [15,16]. VAWTs show a lower cut-in wind speed compared to HAWTs, and considering an average wind speed of 5 m/s and peak values over 7 m/s, VAWTs are more suitable in this context. On the other hand there is no need for wind direction control in VAWTs, so no matter the direction the train is moving, in contrast to the HAWTs.

2.2. PMSG Modelling

Using a direct drive-based permanent magnet synchronous generator (PMSG) significantly improves the reliability of the variable wind turbine, rather than using gear boxes [17–19]. The self-excitation capability of these generators due to permanent magnets, also improves efficiency. However, the variability in wind profiles leads fluctuations in torque of the wind turbine, affecting both in the output voltage and frequency. In order to show the dynamics involving in the generator, mechanical and electrical equations can be summarized as follows:

$$J \cdot \frac{d\omega_m}{dt} - D \cdot \omega_m = T_m - T_e \tag{1}$$

where J is the moment of inertia [kg· m^2], ω_m is the angular speed of the rotor [rad/s], D is the damping constant [Nm/(rad/s)], and T_m and T_e are mechanical and electrical torques applied, respectively. Mechanical power applied to the generator by the VAWT (P_m [W]) can be calculated by the equation defined in (2):

$$P_m = T_m \cdot \omega_m \tag{2}$$

The electrical torque can be defined as shown in (3):

$$T_e = \frac{3}{2} \cdot p \cdot \left(\psi \cdot i_q - \left(L_d - L_q \right) \cdot i_d \cdot i_q \right) \tag{3}$$

where p is the pole pairs of the generator, ψ is the magnetic flux of the permanent magnets $[Wb]$, L_d and L_q are equivalent inductance parameters in direct and quadrature axis, respectively; $[H]$, and i_d and i_q are currents in direct and quadrature axis, respectively, of rotational frame of reference of the rotor $[A]$.

The electrical frequency (ω_e [rad/s]) and mechanical speed are related as follows in (4):

$$\omega_e = p \cdot \omega_m \tag{4}$$

2.3. Diode Bridge and Boost Control: MPPT

As mentioned before, the three-phase voltage magnitude and frequency both depend on the rotational speed of the PMSG. In order to deliver electric power from the generator, it is desirable to generate the maximum power as possible, and there are several ways to do so. A common way to obtain maximum power point from the PMSG, is by using a fully controlled rectifier. However, in this paper, this has been done by using a diode bridge and a boost converter (Figure 2). Using the latter, the efficiency is lower and more harmonics are generated. Anyway, robustness and simplicity of control, which are essential features in small wind turbines, are substantially improved and the costs are lowered [20,21].

The three-phase diode bridge rectifies the alternating current to direct current. However, this voltage is not regulated and in order to get the maximum power, the algorithm has to deal with variables in control.

In order to deliver the maximum power of electric energy generation, maximum power point tracking (MPPT) techniques have been developed in the literature [22–35]. These techniques are broadly categorized into indirect power controller (IPC) and direct power controller (DPC). IPC techniques maximize the captured mechanical wind power, whereas DPC methods directly maximize the electrical power, indeed. Some of these MPPT techniques are listed and compared in Table 1.

Table 1. Comparison of some MPPT techniques.

Algorithm	Complexity	Convergence Speed	Memory Requirement	Wind Speed Measurement	Performance under Varying Wind Conditions	Prior Training/ Knowledge
TSR	Simple	Fast	No	Yes	Moderate	Not required
OT	Simple	Fast	No	No	Moderate	Required
PSF	Simple	Fast	Yes	Yes	Moderate	Required
HCS	Simple	Low	No	No	Moderate	Not required
HCS with FS and AS	High	Medium	No	No	Good	Not required
Modified HCS	High	Fast	No	No	Very good	Not required
INC	Simple	Low	No	No	Moderate	Not required
Modified INC	Medium	Medium	No	No	Good	Not required
ORB	Simple	Medium	No	No	Moderate	Not required
Hybrid	Medium	Fast	No	No	Good	Not required
Fuzzy-based	High	Medium	Yes	Depends	Very good	Required
NN-based	High	Medium	Yes	Depends	Very good	Required
Adaptive	High	Medium	Yes	Depends	Very good	Required
MVPO	High	Low	No	No	Good	Not required

The method used to obtain the maximum power point in this system is the one so called Hill Climb Search (HCS). It is a DPC method, since it uses electrical parameters to obtain the maximum power point. Although the performance of this MPPT technique is moderate, it is very simple both from the point of view of the algorithm and the requirements needed. The amount of current delivered by each boost converter is calculated by measuring input current and voltage (Figure 3). This input current and voltage are multiplied in order to obtain the power. Perturbing the input current set point, the new power is calculated. Considering an increment/decrement in the set point and measuring the increment/decrement of the input power, the set point reaches the maximum power point by climbing the power hill.
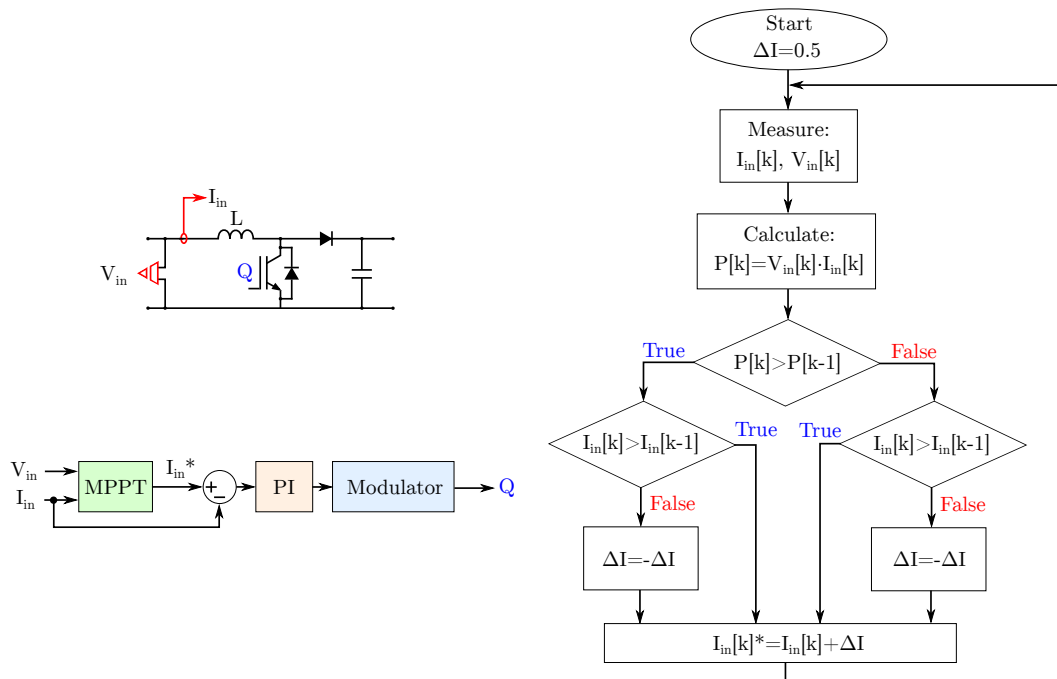
Figure 3. Boost converter, control and Hill Climb Search MPPT algorithm.

3. Converter Parallelization

Considering two sources in parallel supplying a load, there is a need to avoid circulating current between both sources [36–38]. These currents generate undesired losses and fluctuations in the system, so to control the power delivery from paralleled converters there are several techniques [39–44]. Some of these techniques to control paralleled converters are classified in Figure 4.
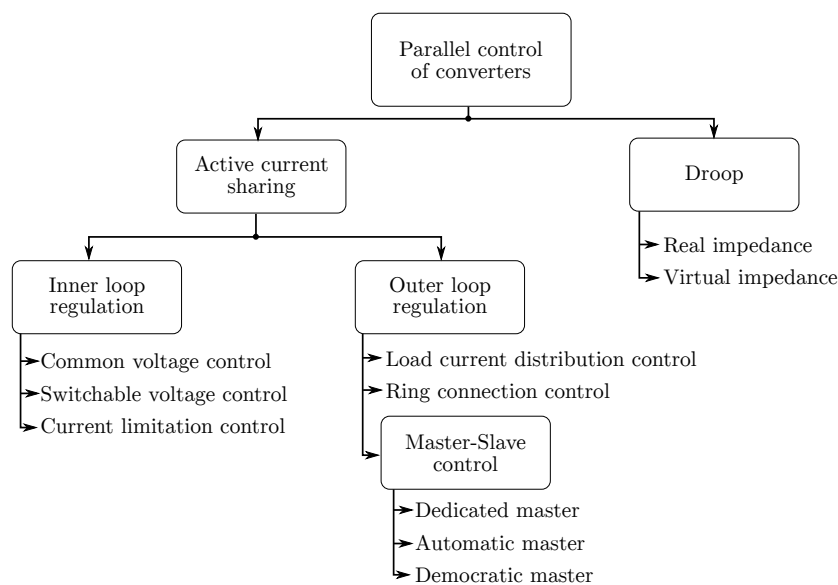

Figure 4. Converter parallelization techniques.

It is important to point out that in DC the parallelization of converters is easier than in AC, due to the lack of wave synchronization both in phase and frequency [41,42].

According to the scenario of this proposal, the DAB is set to master the LVDC bus voltage, so that every wind generator and converter can inject power as a current source to the LVDC bus link. The DAB works as a dedicated voltage master, and the boost converters work as slave in current source mode.

The small scale of the layout of the system allows the master-slave method, which simplifies the control of each converter. For a larger scale attempt, other techniques should be considered.

4. Power Delivery to Catenary: Isolated DAB

In SSTs an isolated dual active bridge (DAB) is a key topology [42,45]. This isolated DAB converter provides a high voltage ratio between low and high voltage sides, ensuring electrical isolation due to the Medium Frequency Transformer (MFT).

An active bridge is connected to the LVDC link, and by controlling the switching devices of the bridge, it is able to provide alternating voltage to the output. This alternating voltage is attached to the low-voltage side of the MFT. The other active bridge DC link is connected to the catenary, and the AC side of the bridge is connected to the high-voltage side of the MFT (Figure 5).
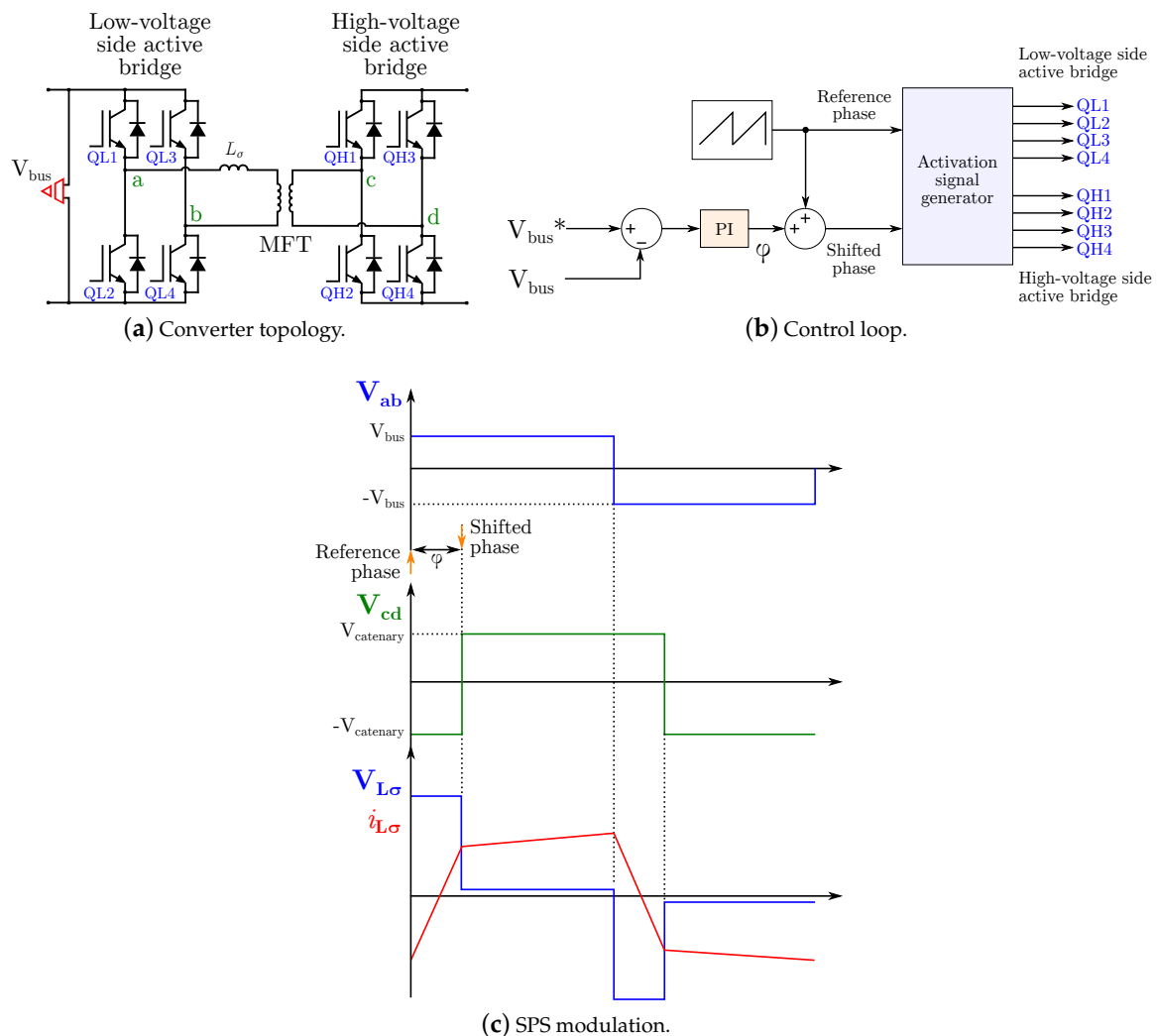

(**a**) Converter topology.

(**b**) Control loop.

(**c**) SPS modulation.

Figure 5. Dual Active Bridge topology, control loop and SPS technique.

The MFTs are made of magnetically soft materials, such as nanocrystal or amorphous [45–48]. These materials show a narrow B-H curve, leading to the reduction in magnetic losses. Moreover, this loss reduction enables the use of a higher switching frequency for the same amount of power, which implies a size reduction as well.

According to modulation techniques, the first one proposed for this type of converters was the Single Phase Shift (SPS) [49]. Square wave signals are generated in both sides of the transformer controlling the switching devices of active bridges, with a phase shift between the two active bridges.

However, many improvements have been carried out adding PWM control to the phase shift control. Complexity has been added in mentioned techniques in order to reduce stress for the parasitic inductance, or to reduce switching losses of devices, among other improvements. In this context, some modulation techniques for the DAB are listed below:

- Single Phase Shift (SPS) [49–51];
- Extented Single Phase Shift (ESPS) [52];
- Dual Phase Shift (DPS) [53,54];
- Triple Phase Shift (TPS) [55,56];
- Hybrid Phase Shift (HPS) [57];
- Triangular Modulation (TRM) [58,59];
- Fundamental Component Analysis (FCA) [60,61];
- Fundamental Duty Modulation (FDM) [62].

In this paper, the SPS has been selected, since it is widely used and easy to implement [53,54,63]. The phase shift magnitude controls the active power flow between both sides of the DAB. In this work, the phase shift is controlled by setting the low side voltage to a DC value of 230 V (Figure 5b).

In the SPS technique, both active bridges work at 50% of duty cycle, generating square waves in the AC side of each bridge. The activation signal generator of the Figure 5b, generates the activation signals for each IGBT in the DAB. The reference phase sets the starting point of one of the square waves, and the other square wave starting point starts phase shifted according to the output of the V_{bus} control. The Medium Frequency Transformer converts voltage ratios, and the inductor is the device which defines the power flow direction. In Figure 5c, the SPS technique is shown according to the phase shift control variable φ. In this context, the controlled loop is the low voltage side bus (LVDC). Setting the LVDC of the DAB, fixes the output voltage of every boost converter, which are connected in parallel. So the DAB works as a master controller for parallel connected slave boost converters, as mentioned earlier. The power flow of the DAB can be calculated as shown in (5).

$$P = \frac{n \cdot V_{bus} \cdot V_{Catenary}}{2 \cdot \pi^2 \cdot f_{SW} \cdot L_\sigma} \cdot \varphi \cdot (\pi - \varphi) \tag{5}$$

where n is the transformation ratio, V_{bus} is the LVDC bus voltage, $V_{Catenary}$ is the MVDC voltage, f_{SW} is the switching frequency of the DAB switching devices, L_σ is the DAB inductance and φ is the phase shift variable control in the SPS technique.

5. Model and Simulation Results

5.1. Simulation Model

The wind energy harnessing system has been modeled in Matlab®/Simulink®. The VAWT, PMSG and the boost converter are shown in Figure 6a, and the SST model is shown in Figure 6b, listing the parameter values in Table 2.

In Figure 6a, the generator and the wind turbine are modeled. The wind turbine parameters behavior has been approximated as the parameters shown by the manufacturer. The control of the boost converter has been as a current source, in order to simplify the parallelization of other boost converters.

In Figure 6b the DAB model and the SPS control are shown. The DAB model reads the V_{bus} and compares with the set point value. Controlling this parameter, the controller outputs a phase shift, which is added to the reference phase for square waves. In this context, the power delivered depends on the generated power by all the generators.

Table 2. Parameters of the model.

Wind turbine	
VAWT	Kliux Zebra 4 kW
Boost converter	
L_{boost}	450 μH
C_{boost}	4.7 mF
f_{SW}	20 kHz
LVDC bus	
C_{bus}	100 mF
SST	
L_σ	200 μH
Transformer	230 V/1500 V
f_{SW}	10 kHz
Catenary	
V_{DC}	1500 V

(**a**) One of the generators and MPPT control.

(**b**) Isolated DAB and SPS control.
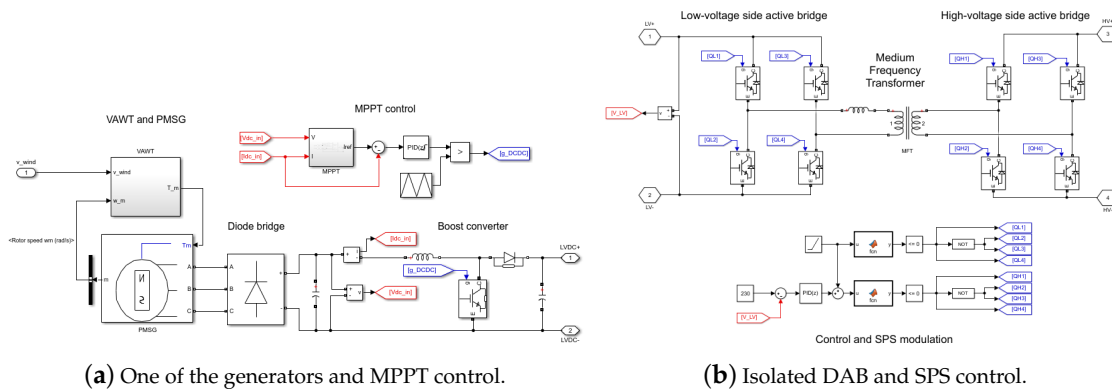
Figure 6. System models.

5.2. Simulation Results

The average wind speed in the location is about 5 m/s without the train going by. Moreover, the wind speed while the train goes by has been simulated in order to estimate it, concluding a maximum wind speed of 7.7 m/s nearby the wind turbine [14]. In Figure 7, the torque and rotational speed of the PMSG during the train displacement are plotted.

The rotational speed of the generator increases as expected. Being rotating before the train goes by, gives an advantage compared to a stopped turbine, since the generator is already delivering power.

The plotted voltage, current and power in Figure 8, tries to show the changes in their value according to the scenario of the train going by. Both the voltage and current change due to the MPPT technique, to extract the maximum power in every instant.

In Figure 9, the electric power generated by two of the sources are compared due to time delay between both of them. In a constant wind speed of 5 m/s, each generator can achieve almost 400 W of power, and while the train goes by, each source is able to generate about 1200 W.
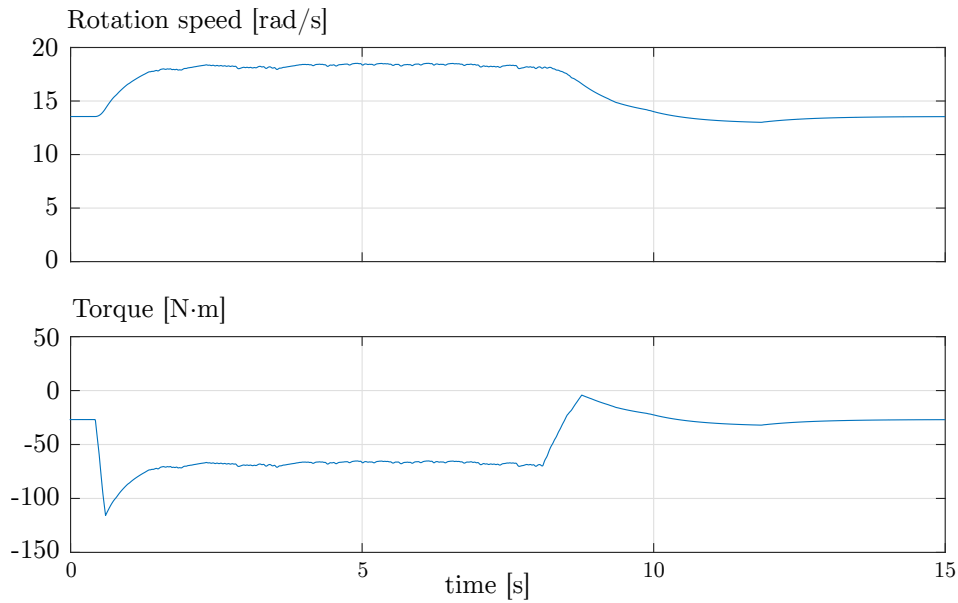
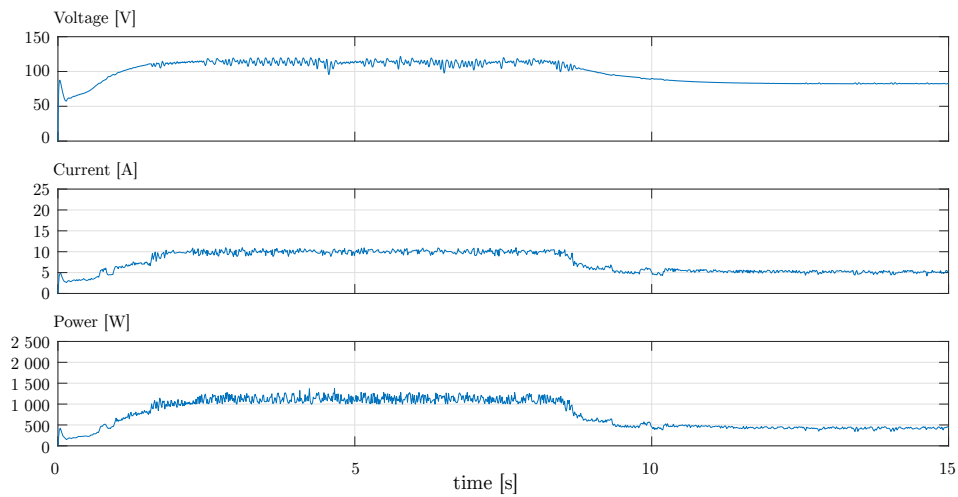**Figure 7.** Torque and rotational speed of the PMSG.

Figure 8. Voltage, current and power at the input of the boost converter.
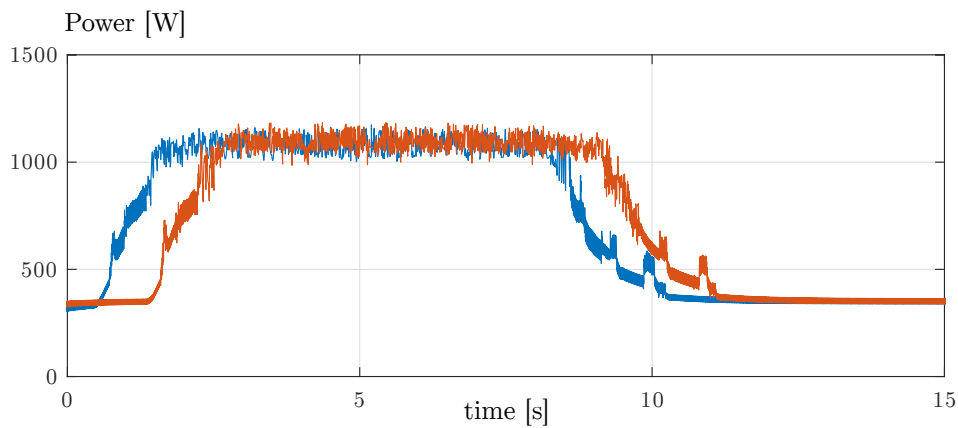
Figure 9. Power generated by two generators along the railway.

The Figure 10 shows the constant bus voltage controlled by the DAB, ensuring the constant value of the LVDC bus voltage even with current injection to it.
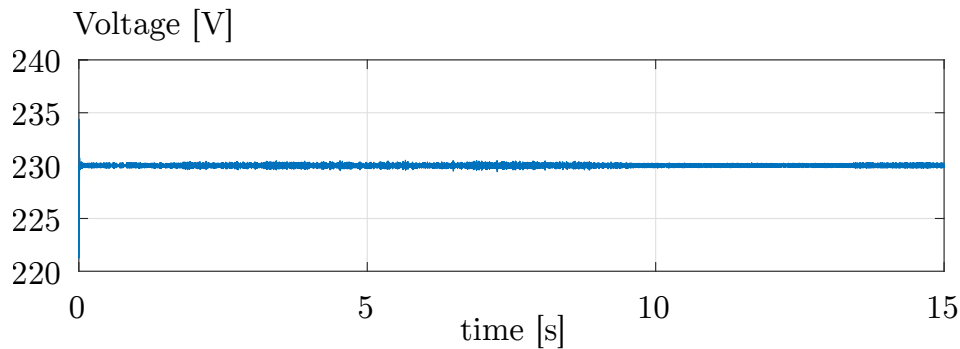
Voltage [V]

Figure 10. LVDC bus voltage.

Finishing with simulation results, the total power delivered to the catenary is plotted in blue in Figure 11, generating up to 11 kW of peak power, and almost 3.5 kW with a constant wind speed of 5 m/s.

In order to show the generated energy data, the wind energy in the location without the wind generated by the train would be about 31 MWh. Taking into account the influence of the train, which can be estimated about 1.33 MWh, the total energy generated could be around 32.3 MWh. This energy is estimated by the simulation results with 10 VAWTs, and as mentioned before, this can be scalable.

5.3. Faulty Scenario

Considering one faulty boost converter, the Figure 11 plots the power delivered of the whole system to the catenary in this conditions.
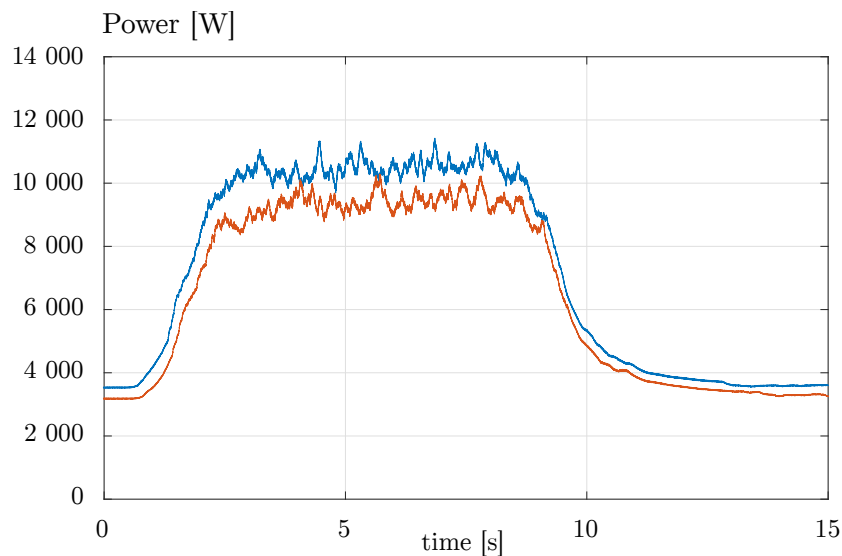
Power [W]

Figure 11. Whole system output power (blue) and with one faulty boost converter (red).

In this faulty condition the energy generated in a whole year would be about 27.9 MWh, and adding up the influence of the train, the total amount of energy would be about 29 MWh. This result shows that the impact of a faulty boost converter is not negligible. However, the system do not present instability in this conditions.

6. Conclusions

This paper proposes a power electronics approach with the aim of empowering the railway infrastructure by connecting several VAWTs nearby the railway to take advantage of both wind and the air mass displacement due to trains. This topology of power conversion is a proof of concept, in which it has been proven that it is feasible and simulations show good results. Research have been

done in order to get MPPT from a wind powered PMSG, also to parallelize DC converters, and the power flow control in a DAB.

As mentioned earlier, this proposal shows an easily scalable control for each generator. Even if one of the MPPT control of a boost converter shows an inadequate behavior, this paper shows that it only affects in the amount of generated power, not in the stability of the whole system.

This proposal also shows the scalability of the whole system with simple boost control, taking advantage of both local wind and the wind generated by the train displacement.

The simulations with 10 VAWTs conclude that this proposal is able to generate about 3.5 kW with the average wind speed, reaching a peak power of 11 kW when the train goes by. In this situation, the system is able to generate 32.3 MWh in a year. The train movement generates almost the 10% of the annual energy. Having a faulty generator, this proposal show that does not affect to the stability of the system, just in delivering lower power to the catenary.

Author Contributions: All authors contributed to the design and implementation of the research, providing critical feedback and helping shape the research, analysis and manuscript. All authors have read and agreed to the published version of the manuscript.

Conflicts of Interest: The authors declare no conflicts of interest.

References

1. IEA. *World Energy Balances 2018*; IEA: Paris, France, 2018.
2. IEA. *Tracking Transport 2020*; IEA: Paris, France, 2020.
3. Falcone, P.M.; Lopolito, A.; Sica, E. The networking dynamics of the Italian biofuel industry in time of crisis: Finding an effective instrument mix for fostering a sustainable energy transition. *Energy Policy* **2018**, *112*, 334–348. [CrossRef]
4. Helliwell, R.; Tomei, J. Practicing stewardship: EU biofuels policy and certification in the UK and Guatemala. *Agric. Hum. Values* **2016**, *34*, 473–484. [CrossRef]
5. Bae, C.; Jang, D.; Kim, Y.; Chang, S.; Mok, J. Calculation of regenerative energy in DC 1500V electric railway substations. In Proceedings of the Internatonal Conference on Power Electronics, Daegu, Korea, 22–26 October 2007; pp. 801–805. [CrossRef]
6. Abril, M.; Barber, F.; Ingolotti, L.; Salido, M.A.; Tormos, P.; Lova, A. An assessment of railway capacity. *Transp. Res. Part E Logist. Transp. Rev.* **2008**, *44*, 774–806. [CrossRef]
7. Falcone, P.M. Analysing stakeholders' perspectives towards a socio-technical change: The energy transition journey in Gela Municipality. *AIMS Energy* **2018**, *6*, 645. [CrossRef]
8. Laskar, M.A.R. Piezoelectricity: An Energy Source for Future Railway Stations. *SEU J. Sci. Eng.* **2017**, *11*. [CrossRef]
9. Baker, C. The flow around high speed trains. *J. Wind Eng. Ind. Aerodyn.* **2010**, *98*, 277–298. [CrossRef]
10. Kwon, H.B.; Park, C.S. An experimental study on the relationship between ballast flying phenomenon and strong wind under high speed train. In Proceedings of the World Congress on Rail Research, Montreal, QC, Canada, 3–6 June 2006.
11. Joshi, S.; Mathur, A.; Jain, A.; Gupta, S.; Jani, N.; Chhabra, B. Generation of electricity using wind energy produced due to the motion of trains. *J. Energy Technol. Policy* **2012**, *2*, 19–23.
12. Kumar, A.; Karandikar, P.; Chavan, D.S. Generating and saving energy by installing wind turbines along the railway tracks. In Proceedings of the 2015 International Conference on Energy Systems and Applications, Pune, India , 30 October–1 November 2015. [CrossRef]
13. Pan, H.; Li, H.; Zhang, T.; Laghari, A.A.; Zhang, Z.; Yuan, Y.; Qian, B. A portable renewable wind energy harvesting system integrated S-rotor and H-rotor for self-powered applications in high-speed railway tunnels. *Energy Convers. Manag.* **2019**, *196*, 56–68. [CrossRef]

14. Asensio, F.J.; San Martín, J.I.; Zamora, I.; Oñederra, O.; Saldaña, G.; Eguia, P. A system approach to harnessing wind energy in a railway infrastructure. In Proceedings of the Annual Conference of the IEEE Industrial Electronics Society (IECON), Washington, DC, USA, 21–23 October 2018; pp. 1646–1651. [CrossRef]

15. Vivek, C.M.; Gopikrishnan, P.; Murugesh, R.; Mohamed, R.R. A review on vertical and horizontal axis wind turbine. *Int. Res. J. Eng. Technol.* **2017**, *4*, 240–250.

16. Battisti, L.; Benini, E.; Brighenti, A.; Dell'Anna, S.; Castelli, M.R. Small wind turbine effectiveness in the urban environment. *Renew. Energy* **2018**, *129*, 102–113. [CrossRef]

17. Li, S.; Haskew, T.A.; Xu, L. Conventional and novel control designs for direct driven PMSG wind turbines. *Electr. Power Syst. Res.* **2010**, *80*, 328–338. [CrossRef]

18. Shehata, E.G. A comparative study of current control schemes for a direct-driven PMSG wind energy generation system. *Electr. Power Syst. Res.* **2017**, *143*, 197–205. [CrossRef]

19. Devashish, T.A. A comprehensive review on wind energy system for electric power generation: Current situation and improved technologies to realize future development. *Int. J. Renew. Energy Res.* **2017**, *7*, 1786–1805.

20. Urtasun, A.; Sanchis, P.; Martín, I.S.; López, J.; Marroyo, L. Modeling of small wind turbines based on PMSG with diode bridge for sensorless maximum power tracking. *Renew. Energy* **2013**, *55*, 138–149. [CrossRef]

21. Baroudi, J.A.; Dinavahi, V.; Knight, A.M. A review of power converter topologies for wind generators. *Renew. Energy* **2007**, *32*, 2369–2385. [CrossRef]

22. Kumar, D.; Chatterjee, K. A review of conventional and advanced MPPT algorithms for wind energy systems. *Renew. Sustain. Energy Rev.* **2016**, *55*, 957–970. [CrossRef]

23. Kumar, M.B.H.; Saravanan, B.; Sanjeevikumar, P.; Blaabjerg, F. Review on control techniques and methodologies for maximum power extraction from wind energy systems. *IET Renew. Power Gener.* **2018**, *12*, 1609–1622. [CrossRef]

24. Abdullah, M.; Yatim, A.; Tan, C.; Saidur, R. A review of maximum power point tracking algorithms for wind energy systems. *Renew. Sustain. Energy Rev.* **2012**, *16*, 3220–3227. [CrossRef]

25. Kot, R.; Rolak, M.; Malinowski, M. Comparison of maximum peak power tracking algorithms for a small wind turbine. *Math. Comput. Simul.* **2013**, *91*, 29–40. [CrossRef]

26. Cheng, M.; Zhu, Y. The state of the art of wind energy conversion systems and technologies: A review. *Energy Convers. Manag.* **2014**, *88*, 332–347. [CrossRef]

27. Menezes, E.J.N.; Araújo, A.M.; da Silva, N.S.B. A review on wind turbine control and its associated methods. *J. Clean. Prod.* **2018**, *174*, 945–953. [CrossRef]

28. Sarkar, J.; Khule, S.S. A study of MPPT schemes in PMSG based wind turbine system. In Proceedings of the International Conference on Electrical, Electronics, and Optimization Techniques (ICEEOT), Chennai, India, 3–5 March 2016; pp. 100–105. [CrossRef]

29. Nasiri, M.; Milimonfared, J.; Fathi, S.H. Modeling, analysis and comparison of TSR and OTC methods for MPPT and power smoothing in permanent magnet synchronous generator-based wind turbines. *Energy Convers. Manag.* **2014**, *86*, 892–900. [CrossRef]

30. Wei, C.; Zhang, Z.; Qiao, W.; Qu, L. An adaptive network-based reinforcement learning method for MPPT control of PMSG wind energy conversion systems. *IEEE Trans. Power Electron.* **2016**, *31*, 7837–7848. [CrossRef]

31. Dalala, Z.M.; Zahid, Z.U.; Yu, W.; Cho, Y.; Lai, J. Design and analysis of an MPPT technique for small-scale wind energy conversion systems. *IEEE Trans. Energy Convers.* **2013**, *28*, 756–767. [CrossRef]

32. Llano, D.X.; McMahon, R.A. Control techniques with system efficiency comparison for microwind turbines. *IEEE Trans. Sustain. Energy* **2017**, *8*, 1609–1617. [CrossRef]

33. Jeong, H.G.; Seung, R.H.; Lee, K.B. An Improved Maximum Power Point Tracking Method for Wind Power Systems. *Energies* **2012**, *5*, 1339–1354. [CrossRef]

34. Kolesnik, S.; Kuperman, A. Analytical Derivation of Electrical-Side Maximum Power Line for Wind Generators. *Energies* **2017**, *10*, 1498. [CrossRef]

35. Syahputra, R.; Soesanti, I. Performance Improvement for Small-Scale Wind Turbine System Based on Maximum Power Point Tracking Control. *Energies* **2019**, *12*, 3938. [CrossRef]

36. Augustine, S.; Mishra, M.K.; Lakshminarasamma, N. Circulating current minimization and current sharing control of parallel boost converters based on droop index. In Proceedings of the IEEE International Symposium on Diagnostics for Electric Machines, Power Electronics and Drives (SDEMPED), Valencia, Spain, 27–30 August 2013; pp. 454–460. [CrossRef]

37. Dragičević, T.; Lu, X.; Vasquez, J.C.; Guerrero, J.M. DC Microgrids—Part I: A Review of Control Strategies and Stabilization Techniques. *IEEE Trans. Power Electron.* **2016**, *31*, 4876–4891.

38. Zheng, X.; Ali, H.; Wu, X.; Zaman, H.; Khan, S. Non-Linear Behavioral Modeling for DC-DC Converters and Dynamic Analysis of Distributed Energy Systems. *Energies* **2017**, *10*, 63. [CrossRef]

39. Gao, F.; Bozhko, S.; Costabeber, A.; Patel, C.; Wheeler, P.; Hill, C.I.; Asher, G. Comparative stability analysis of droop control approaches in voltage-source-converter-based DC microgrids. *IEEE Trans. Power Electron.* **2016**, *32*, 2395–2415. [CrossRef]

40. Chiang, H.; Jen, K.; You, G. Improved droop control method with precise current sharing and voltage regulation. *IET Power Electron.* **2016**, *9*, 789–800. [CrossRef]

41. Huang, Y.; Tse, C.K. Circuit theoretic classification of parallel connected DC-DC converters. *IEEE Trans. Circuits Syst. I Regul. Pap.* **2007**, *54*, 1099–1108. [CrossRef]

42. Freijedo, F.D.; Rodriguez-Diaz, E.; Dujic, D. Stable and passive high-power dual active bridge converters interfacing MVDC grids. *IEEE Trans. Ind. Electron.* **2018**, *65*, 9561–9570. [CrossRef]

43. Xiong, F.; Wu, J.; Hao, L.; Liu, Z. Backflow Power Optimization Control for Dual Active Bridge DC-DC Converters. *Energies* **2017**, *10*, 1403. [CrossRef]

44. Vazquez, A.; Martin, K.; Arias, M.; Sebastian, J. On Bidirectional DC Nano-Grids: Design Considerations and an Architecture Proposal. *Energies* **2019**, *12*, 3715. [CrossRef]

45. Yuan, L.; Lu, Z.; Sun, J.; Duan, R.; Zhao, Z. Comparative evaluation of isolated bidirectional DC/DC converter in high-power high-frequency occasions. In Proceedings of the International Conference on Electrical Machines and Systems (ICEMS), Jeju, Korea, 7–10 October 2018. [CrossRef]

46. Samejima, T.; Kintsu, K.; Morizane, T.; Kimura, N. Comparison of core material of high frequency transformer for offshore wind generation. In Proceedings of the International Symposium on Power Electronics, Electrical Drives, Automation and Motion (SPEEDAM), Amalfi, Italy, 20–22 June 2018. [CrossRef]

47. Yeh, C.S.; Lai, J.S. A study on high frequency transformer design in medium-voltage solid-state transformers. In Proceedings of the Asian Conference on Energy, Power and Transportation Electrification (ACEPT), Singapore, 30 October–2 November 2018. [CrossRef]

48. Sarker, P.C.; Islam, M.R.; Guo, Y.; Zhu, J.; Lu, H.Y. State-of-the-art technologies for development of high frequency transformers with advanced magnetic materials. *IEEE Trans. Appl. Supercond.* **2019**, *29*, 1–11. [CrossRef]

49. Doncker, R.W.A.A.D.; Divan, D.M.; Kheraluwala, M.H. A three-phase soft-switched high-power-density DC/DC converter for high-power applications. *IEEE Trans. Ind. Appl.* **1991**, *27*, 63–73. [CrossRef]

50. Qin, H.; Kimball, J.W. Closed-loop control of DC–DC dual-active-bridge converters driving single-phase inverters. *IEEE Trans. Power Electron.* **2014**, *29*, 1006–1017. [CrossRef]

51. Song, W.; Hou, N.; Wu, M. Virtual direct power control scheme of dual active bridge DC–DC converters for fast dynamic response. *IEEE Trans. Power Electron.* **2018**, *33*, 1750–1759. [CrossRef]

52. Zhao, B.; Yu, Q.; Sun, W. Extended-phase-shift control of isolated bidirectional DC–DC converter for power distribution in microgrid. *IEEE Trans. Power Electron.* **2012**, *27*, 4667–4680. [CrossRef]

53. Karthikeyan, V.; Gupta, R. Closed-loop control of isolated dual active bridge converter using dual phase shift modulation. In Proceedings of the Annual Conference of the IEEE Industrial Electronics Society (IECON), Yokohama, Japan, 9–12 November 2015. [CrossRef]

54. Bai, H.; Mi, C. Eliminate reactive power and increase system efficiency of isolated bidirectional dual-active-bridge DC–DC converters using novel dual-phase-shift control. *IEEE Trans. Power Electron.* **2008**, *23*, 2905–2914. [CrossRef]

55. Wu, K.; de Silva, C.W.; Dunford, W.G. Stability analysis of isolated bidirectional dual active full-bridge DC–DC converter with triple phase-shift control. *IEEE Trans. Power Electron.* **2012**, *27*, 2007–2017. [CrossRef]

56. Calderon, C.; Barrado, A.; Rodriguez, A.; Alou, P.; Lazaro, A.; Fernandez, C.; Zumel, P. General Analysis of Switching Modes in a Dual Active Bridge with Triple Phase Shift Modulation. *Energies* **2018**, *11*, 2419. [CrossRef]

57. Zhou, H.; Khambadkone, A.M. Hybrid modulation for dual-active-bridge bidirectional converter with extended power range for ultracapacitor application. *IEEE Trans. Ind. Appl.* **2009**, *45*, 1434–1442. [CrossRef]

58. Jauch, F.; Biela, J. Generalized modeling and optimization of a bidirectional dual active bridge DC-DC converter including frequency variation. In Proceedings of the International Power Electronics Conference (IPEC), Hiroshima, Japan, 18–21 May 2014. [CrossRef]

59. Krismer, F.; Round, S.; Kolar, J.W. Performance optimization of a high current dual active bridge with a wide operating voltage range. In Proceedings of the IEEE Power Electronics Specialists Conference, Jeju, Korea, 18–22 June 2006. [CrossRef]

60. ichi Itoh, J.; Higa, H.; Nagano, T. A novel control method focusing on reactive power for a dual active bridge converter. In Proceedings of the International Power Electronics and Application Conference and Exposition, Shanghai, China, 5–8 November 2014. [CrossRef]

61. Zhao, B.; Song, Q.; Liu, W.; Liu, G.; Zhao, Y. Universal high-frequency-link characterization and practical fundamental-optimal strategy for dual-active-bridge DC-DC converter under PWM plus phase-shift control. *IEEE Trans. Power Electron.* **2015**, *30*, 6488–6494. [CrossRef]

62. Choi, W.; Rho, K.M.; Cho, B.H. Fundamental duty modulation of dual-active-bridge converter for wide-range operation. *IEEE Trans. Power Electron.* **2016**, *31*, 4048–4064. [CrossRef]

63. Shi, L.; Lei, W.; Li, Z.; Cui, Y.; Huang, J.; Wang, Y. Stability analysis of digitally controlled dual active bridge converters. *J. Mod. Power Syst. Clean Energy* **2017**, *6*, 375–383. [CrossRef]